Analytic-Wavelet-Ridge-Based Detection of Dynamic Eccentricity in Brushless Direct Current (BLDC) Motors Functioning Under Dynamic Operating Conditions

Satish Rajagopalan, *Member, IEEE*, José M. Aller, José A. Restrepo, *Member, IEEE*, Thomas G. Habetler, *Fellow, IEEE*, and Ronald G. Harley, *Fellow, IEEE*

***Abstract*—A new method using the analytic wavelet transform of the stator-current signal is proposed for detecting dynamic eccentricity in brushless direct current (BLDC) motors operating under rapidly varying speed and load conditions. As wavelets are inherently suited for nonstationary signal analysis, this method does not require the use of any windows, nor is it dependent on any assumption of local stationarity as in the case of the short-time Fourier transform. The proposed technique uses analytic wavelets, which are smooth wavelets that possess both magnitude and phase information. This makes them particularly suitable for motor-fault diagnostics. Experimental results are provided to show that the proposed method works over a wide speed range of motor operation and provides an effective and robust way of detecting rotor faults such as dynamic eccentricity in BLDC motors.**

***Index Terms*—Brushless direct current (BLDC) motor, condition monitoring, dynamic eccentricity, dynamic operation, fault diagnosis, nonstationary, rotor faults, wavelets.**

I. Introduction

BRUSHLESS direct current (BLDC) motors are rapidly gaining popularity and are now widely used in industries such as appliances, automotive, aerospace, consumer, medical, industrial automation equipment, and instrumentation. As the name implies, BLDC motors do not use brushes for commutation; instead, they are electronically commutated. They have many advantages over brushed dc motors and induction motors. A few of these are better speed versus torque characteristics, higher dynamic response, higher efficiency, and noiseless operation. In addition, the ratio of torque that is delivered to the size of the motor is higher, making it useful in applications where space and weight are critical factors [1]. More BLDC machines are therefore being used, often in critical high-performance applications. Fault diagnosis and condition monitoring of BLDC machines is therefore assuming a new importance. Early detection of faults and asymmetries would allow preventive maintenance to be performed and provide sufficient time for controlled shutdown of the process, thereby reducing the costs of outage time and repairs. The range of faults that could occur in BLDC machines includes stator faults, rotor faults, and inverter faults.

Diagnostics of electrical motors operating under constant speed conditions has been well investigated in literature [2]–[4]. The fundamental assumption of stationarity in constant-speed operation allows the use of the well-known method of Fourier transformation in the frequency analysis of currents, voltages, and vibration signals to detect various rotor and mechanical faults in an electrical machine. However, there are several applications where the motor is never operating at a constant speed or load. A motor operating in such a nonstationary environment has a nonstationary voltage, current, and vibration signal. The term nonstationary in signal processing literature is usually described statistically [5]. However, from an electric motor's operating point of view, this simply refers to an operation where the motor's state variables continuously change with time, and the motor is never operating at a constant speed throughout its operation. Some attempts have been made to detect machine faults in motors operating under different cases of slowly varying load and speed conditions. Yazici and Kliman [6] use short-time Fourier transforms (STFTs) and pattern-recognition techniques to detect faults in induction motors under varying operating conditions. Their application is however based on the assumption that the change in speed and load occurs very slowly and there are sufficiently long intervals of time wherein the motor can be assumed to operate in a stationary condition. This is common in applications such as rolling steel mills and in the cement industry. Another approach to a similar application that uses wavelets is presented in [7]. Another area where nonstationary signal analysis has been attempted is the diagnosis of machine faults from the starting current transients in induction motors. This enables the detection of faults under no-load condition where the only measurable and useful current exists during the starting of the motor and is in a transient

Manuscript received May 24, 2006; revised November 13, 2006. This work was supported by Duke Power Company, Charlotte, NC. This paper was presented in part at the 31st Annual Conference of the IEEE Industrial Electronics Society, Raleigh, NC, November 6–10, 2006.

S. Rajagopalan was with the School of Electrical and Computer Engineering, Georgia Institute of Technology, Atlanta, GA 30332 USA. He is now with the Power Delivery Group, Electric Power Research Institute, Knoxville, TN 37923 USA (e-mail: satish.r@ieee.org; srajagopalan@epri.com).

J. M. Aller and J. A. Restrepo are with the Departamento de Conversión y Transporte de Energía, Universidad Simón Bolívar, Caracas 1080-A, Venezuela (e-mail: jaller@usb.ve; restrepo@usb.ve).

T. G. Habetler and R. G. Harley are with the School of Electrical and Computer Engineering, Georgia Institute of Technology, Atlanta, GA 30332 USA (e-mail: thabetler@ee.gatech.edu; ron.harley@ece.gatech.edu).

Digital Object Identifier 10.1109/TIE.2007.894699

state [8], [9]. However, none of these methods attempts to diagnose faults in applications where the motor is continuously in a nonstationary stage or where assumptions of local or slow stationarity may be questionable and unrealistic.

A novel analytic-wavelet-transform (AWT)-based detector for tracking rotor faults such as dynamic eccentricity in BLDC motors is proposed in this paper. The proposed method extracts the rotor-fault frequencies from the stator current of the BLDC motor using AWT. A ridge detector is then applied to track the maxima of the wavelet-extracted fault frequencies over time, thus providing a method to detect rotor faults in motors operating under nonstationary conditions.

II. Need for Analytic Wavelets and Ridge Detection

The analysis of rapid time-varying signals requires detection of time-varying events as well as identification of the behavior of the signal over a length of time. One method that is commonly used to achieve this is STFT where a short length of the signal is analyzed at a time. The use of a single analysis window is thus a compromise between time and frequency resolutions. However, in wavelet analysis, a signal is analyzed at different scales or resolutions: A large window is used to look at the approximate stationarity of the signal, and a small window is simultaneously used to look for transients. This multiresolution or multiscale view of the signal forms the foundation for wavelet analysis [10]. The wavelet analysis is performed using a single prototype function called a wavelet. This function is analogous to the sine function that is used in Fourier transforms but is structured to suit transient applications. Fine temporal analysis is performed using the compressed version (high frequency) of the wavelet, while fine frequency analysis uses dilated versions (low frequency) of the wavelet [10]. The wavelet transform decomposes signals over dilated and translated wavelets. A wavelet is a function ψ with a zero average [11], i.e.,

$$\int_{-\infty}^{+\infty} \psi(t)dt = 0. \tag{1}$$

It is normalized to $\|\psi\| = 1$ and centered in the neighborhood of $t = 0$. A family of time-frequency atoms is obtained by scaling ψ by s and translating it by u, i.e.,

$$\psi_{u,s}(t) = \frac{1}{\sqrt{s}}\psi\left(\frac{t-u}{s}\right). \tag{2}$$

The wavelet transform of signal $f(t)$ at time u and scale s is given by

$$Wf(u,s) = \langle f, \psi_{u,s}\rangle = \int_{-\infty}^{+\infty} f(t)\frac{1}{\sqrt{s}}\psi^*\left(\frac{t-u}{s}\right)dt. \tag{3}$$

The energy density of the signal is then represented by scalogram $P_W f$, which is defined as

$$P_W f(u,\xi) = |Wf(u,s)|^2 \tag{4}$$

where $\xi = \eta/s$ is the center frequency of the scaled wavelet $\psi_{u,s}$ and η is the center frequency of the original mother wavelet ψ [10].

In motor diagnostics, the motor health can be evaluated by monitoring the frequency spectrum of the stator current over time. This application therefore possesses two key requirements from a wavelet standpoint.

1) The frequency information is essential to fault diagnostics and must be extracted from the stator-current signal.
2) Moreover, the fault frequencies are smooth (sinusoidal) quantities and do not occur as sharp transient events. Hence, any wavelet that is chosen for this application must be able to approximate such smooth quantities.

A real wavelet (e.g., Mexican-hat wavelet) does not possess separate phase information and hence is suitable only for detecting sharp transients [11]. However, a complex analytic wavelet can separate amplitude and phase components from a signal and can be used to measure instantaneous frequencies, as will be explained in detail in this paper. The analytic wavelet is, therefore, chosen for this application.

Another key challenge that is faced in motor diagnostics is the small amplitude of fault frequencies, which are typically less than 1% of the fundamental amplitude. Even with filtering of the fundamental component, interference that is caused by noise, ghosts, and other artifacts cannot be ignored, and some of these components may be comparable in magnitude to the fault frequencies. Hence, a simple scalogram of the filtered stator current does not suffice, as this scalogram would also reveal these strong nonfault-frequency components that have to be separated from the fault/inverter frequencies. The phase information that is provided by the complex analytic wavelet helps in tracking only genuine frequency components of the stator current while ignoring most of the other artifacts. This method termed as "analytic-wavelet-ridge detection" will be explained in the next section.

III. Analytic Wavelet Ridges

AWT is calculated by using analytic wavelet ψ in (3). Its time-frequency resolution depends on the time-frequency spread of the wavelet atoms $\psi_{u,s}$. Analytic wavelet $\psi(t)$ can be constructed by modulating frequency $(\exp(i\eta t))$ with a real and symmetric window $g(t)$ as in

$$\psi(t) = g(t)e^{i\eta t}. \tag{5}$$

A common analytic wavelet is the Gabor wavelet. It is obtained by frequency modulating a Gaussian window with a complex exponential, as shown in (5). Mathematically, the Gabor wavelet can be expressed as

$$g(t) = \frac{1}{(\sigma^2\pi)^{1/4}}e^{-\frac{t^2}{2\sigma^2}} \tag{6}$$

where σ^2 is the variance. The Gaussian window has the additional advantage of offering the most optimum combination of time and frequency resolutions, as the uncertainty theorem can be used to show that the area of a Heisenberg box reaches the minimum value of 1/2 only for a Gaussian function.

A more detailed treatment of this subject is available in [11]. The Fourier transform of this window is

$$\hat{g}(\omega) = (4\pi\sigma^2)^{1/4} e^{-\frac{\sigma^2\omega^2}{2}} \tag{7}$$

where ω is the instantaneous frequency. If $\sigma^2\eta^2 \gg 1$, then $\hat{g}(\omega) \sim 0$ for $|\omega| > \eta$. Such Gabor wavelets are thus considered to be approximately analytic [11].

Approximate analytic wavelets have some negative frequency components as the Fourier transform of these wavelets may not be exactly zero at negative frequency. This may cause some additional interference components.

The instantaneous frequencies f in the signal are measured from the ridges of the normalized form of the scalogram $P_W f$, which is computed using the analytic wavelet. The instantaneous frequency is defined as a positive derivative $\varphi'(t)$ of phase $\varphi(t)$ of the respective spectral component. The normalized scalogram is defined by

$$\frac{\xi}{\eta} P_W f(u,\xi) = \frac{|Wf(u,s)|^2}{s} \tag{8}$$

for $\xi = \eta/s$.

Without going into the mathematical details of the derivation (further details are available in [11, pp. 103–104]), the AWT of a sinusoidal function $f(t) = a(t)\cos(\varphi(t))$ is given as

$$Wf(u,s) = \frac{\sqrt{s}}{2} a(u) \exp\left[i\varphi(u)\right] \left(\hat{g}\left(s\left[\xi - \varphi'(u)\right]\right)\right). \tag{9}$$

The phase information of the AWT in (9) is now used to calculate the wavelet ridges. Equation (9) shows that the scalogram is maximum at [11]

$$\frac{\eta}{s(u)} = \xi(u) = \varphi'(u). \tag{10}$$

The corresponding points $(u, \xi(u))$ are called wavelet ridges. The complex phase of $Wf(u,s)$ in (9) is given as

$$\Phi_W(u,\xi) = \varphi(u). \tag{11}$$

At ridge points,

$$\frac{\partial \Phi_W(u,\xi)}{\partial u} = \varphi'(u) = \xi. \tag{12}$$

Thus, the ridges are the local maxima of the scalogram and are frequency components that essentially have a stationary phase. Equation (12) eliminates noise, ghosts, and other artifacts as these do not satisfy this condition. Thus, only the instantaneous frequencies that match the positive derivative of the phase are chosen, and the other frequencies are discarded.

In multicomponent signals that have more than one frequency, the instantaneous frequencies can be discriminated as long as bandwidth relations (13) and (14) are satisfied [11], i.e.,

$$\frac{\left|\varphi_i'(u) - \varphi_j'(u)\right|}{\varphi_i'(u)} \geq \frac{\Delta\omega}{\eta} \tag{13}$$

$$\frac{\left|\varphi_i'(u) - \varphi_j'(u)\right|}{\varphi_j'(u)} \geq \frac{\Delta\omega}{\eta} \tag{14}$$

where $\Delta\omega$ is the bandwidth of $\hat{g}(\omega)$ and φ_i and φ_j are any two frequency components in the given signal. Equations (13) and (14) are used to select the center frequency for the wavelet. AWT can be implemented to operate in real time and integrated into a motor drive system using a simple and fast method based on the well-known fast Fourier transform (FFT) [12].

IV. Dynamic Eccentricity in BLDC Motors

Rotor faults in BLDC machines are usually comprised of eccentricities (dynamic and static) and chipped rotor magnets [13]. Machine eccentricity is the condition of unequal air gap that exists between the stator and the rotor. Air-gap eccentricity can occur in the form of static or dynamic eccentricity. In the case of static eccentricity, the position of minimum radial air-gap length is fixed in space. Typical causes of static eccentricity include stator core ovality or incorrect positioning of the rotor or the stator at assembly stage. Dynamic eccentricity occurs when the center of the rotor is not at the center of rotation and the minimum air gap revolves with the rotor. This means that dynamic eccentricity is a function of space and time. Typical causes of dynamic eccentricity include bent shaft, mechanical resonances, and bearing wear.

When eccentricity becomes large, the resulting unbalanced radial forces [also known as unbalanced magnetic pull (UMP)] can cause stator-to-rotor rub, and this can result in damage to the stator and the rotor [3]. In the case of static eccentricity, this is a steady pull in one direction. This makes the UMP difficult to detect unless specialized equipment is used, which is impractical for motors in service [4]. Dynamic eccentricity, on the other hand, produces a UMP that rotates at the mechanical speed of the motor and acts directly on the rotor. This makes the UMP easier to detect by vibration or current monitoring. Due to this reason, dynamic-eccentricity detection is the main focus of this paper. The proposed method can also be used for detecting other faults such as load (gear) faults, misalignments, and bearing faults that also produce unique fault-frequency signature components in the stator current, which is similar to the dynamic-eccentricity fault. However, these faults are not considered in this paper as it is complex task to practically recreate many of these faults in a laboratory environment.

Fault detection in induction motors operating under steady-state condition has been investigated for quite some time, and the most well-known method is through the detection of unique fault signatures in the motor stator current. This method known as motor current signature analysis (MCSA) and several of its variations continue to be used in the detection of motor faults in induction motors operating operate under constant speed and load conditions [14]–[17]. In addition to monitoring electrical current, motor faults can also be detected by monitoring the electromagnetic torque spectrum. An analysis of current- and torque-based induction-motor fault detection is provided in [18].

Rajagopalan *et al.* [13] have extended the concept of MCSA to permanent-magnet machines and have shown that dynamic eccentricity in BLDC motors operating at a constant speed affect certain characteristic frequency components in the machine stator current. The rotor defect can, therefore, be identified by

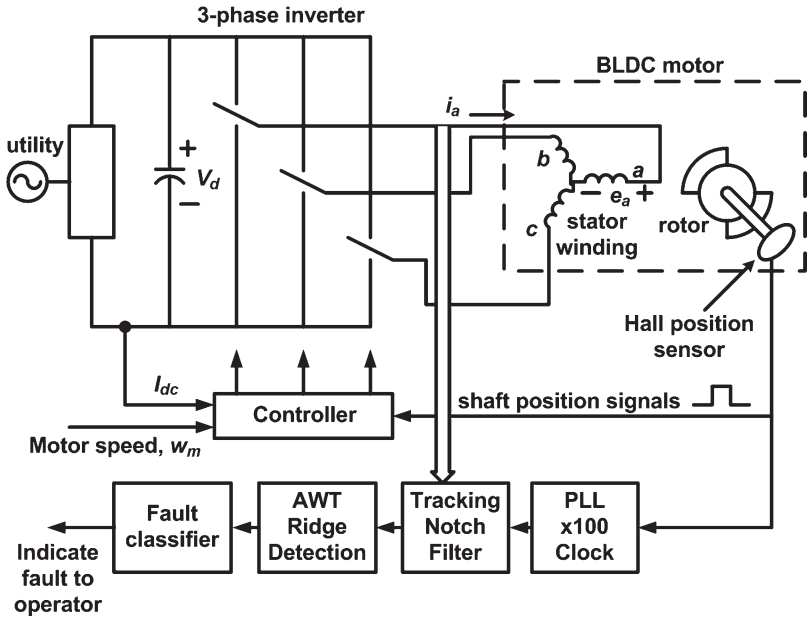

Fig. 1. AWT-ridge-based BLDC rotor-fault detector.

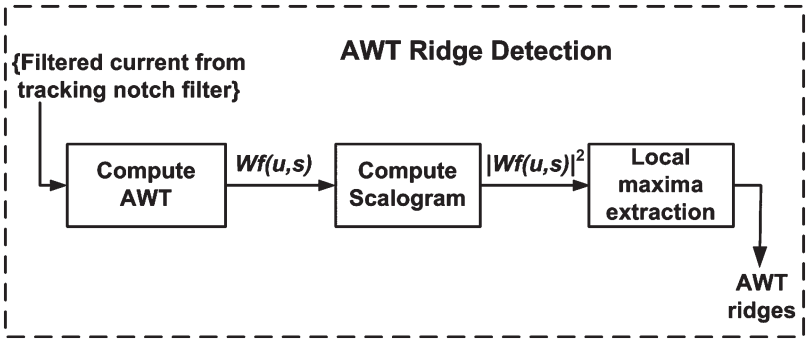

Fig. 2. AWT-ridge-detection algorithm.

monitoring the amplitude of these harmonic components [13]. The frequency spectrum of the stator current is computed using FFT [14]. The rotor-fault frequencies are then identified from the current spectrum and monitored to detect the severity of the fault. Dynamic eccentricity in BLDC motors causes current components at frequencies given by [13]

$$f_{rf} = f_e \pm k\frac{f_e}{P/2} \tag{15}$$

where f_{rf} is the rotor-fault frequency, f_e is the fundamental frequency, P is the number of poles in the BLDC machine, and k is any integer. These fault frequencies are also present when the BLDC stator current is in a nonstationary state. The health of the BLDC motor can be diagnosed by monitoring these fault frequencies.

V. AWT-Ridge-Based BLDC Rotor-Fault-Detection Algorithm

The AWT-ridge-based BLDC fault-detection strategy for detecting dynamic eccentricities in a BLDC motor is shown in Fig. 1. The figure shows a BLDC motor that is driven by an inverter. One of the stator phase currents is sensed. The sampled stator current is adaptively filtered using a tracking notch filter to remove the fundamental and all harmonics that are above the second harmonic. This notch filter can be a switch-capacitor filter as used in this paper. This adaptive filtering is needed as the stator current is nonstationary. The structure of this filter is explained in the next section. Once the filtered current is obtained, the AWT ridges are extracted. This process is shown in more detail in Fig. 2. Once, the ridges are extracted, fault classification is done based on their instantaneous amplitudes.

Referring to Fig. 2, the AWT with Gabor wavelet is first computed from the adaptively filtered current signal using (3) and (6). The scalogram is then computed from the AWT using (4). A discrete version of the AWT is used since it is difficult and impractical to calculate the continuous AWT of (3). The computation of the continuous AWT in (3) assumes that the AWT is calculated for all values of the scale, i.e., s, from zero to infinity. However, this is not practically possible. In practice, the AWT is calculated for a range of predetermined scales s. For example, the discrete wavelet transform (AWT that is computed at discrete scale intervals of s) is usually computed at scales $s = q^j$, with $q = 2^{1/v}$, which provides v intermediate scales in each octave, i.e., $[2^j, 2^{j+1})$ [11]. The choice of the number

of intermediate scales is determined based on the accuracy of computation that is desired. It is usually chosen to be the largest that is permissible from a computational aspect and is selected based on the processor that is used for implementing the diagnostic algorithm. The error that is introduced by the discretization process decreases as the number of intermediate scales v is increased.

The instantaneous fault frequencies are then extracted from the scalogram by using the wavelet ridge algorithm. As shown in Fig. 2, this is done by locating the maxima of the scalogram over time. The wavelet ridges are the instantaneous local maxima of the scalogram that also possess stationary phase characteristics, as explained previously, and can be checked by using the complex phase information that is obtained from the AWT as that in (12). Frequencies that do not have a stationary phase are discarded.

A simple fault metric is used to detect the fault by calculating the rms value of the instantaneous amplitudes of the fault ridges and is given by

$$\text{rms fault metric} = \sqrt{\frac{1}{N_r}\sum_{i=1}^{i=N_r} f_i^2(t)} \tag{16}$$

where $f_i(t)$ is the amplitude of the instantaneous rotor-fault frequencies that are extracted from the spectrogram of the filtered current using the ridge algorithm. The N_r in (16) corresponds to the number of Fourier ridge frequencies that are extracted at any given time. This metric is used to indicate a developing rotor fault. A heuristically set threshold classifies the motor as good or bad. The rms metric in (16) is sufficient for the work that is reported in this paper as only one fault is investigated, with the objective of this paper being the demonstration of the viability of nonstationary motor diagnostics using analytic wavelets. However, in the event of actual condition monitoring, several faults may be encountered. In such cases, all the amplitudes of all the fault frequencies have to be individually monitored to determine the type of fault.

VI. Experimental Arrangement

A six-pole 12-V 1-kW BLDC motor is used to implement dynamic eccentricity. The BLDC motor has a current control loop and a speed control loop. Dynamic eccentricity is implemented by first removing the bearing from the rotor shaft. In a machine shop, some material is removed from one side of the rotor shaft at one end of the motor, and the rotor is then placed back onto the bearing. Shims are now inserted between the bearing and the shaft on the side that is opposite to where the material was removed, as shown in Fig. 3, thus pushing the center of rotation of the rotor away from the center of the stator. The original length of the air gap was 0.75 mm, and the rotor is now shifted by approximately 0.25 mm (32% of the normal air-gap length) from its center by inserting a steel shim with a thickness of 0.001 in ($\sim$0.25 mm). The defect that is induced in this manner represents a realistic dynamic-eccentricity fault that can occur during normal motor operation. Typical eccentricity tolerances during motor manufacture can vary over a range of 5%–20% of

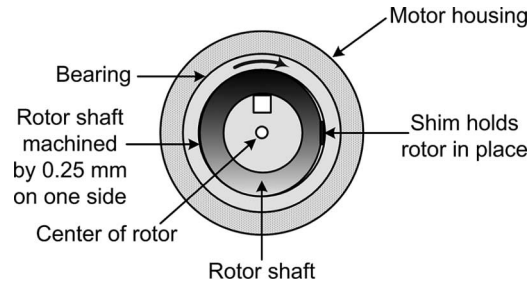

Fig. 3. Implementation of dynamic eccentricity.

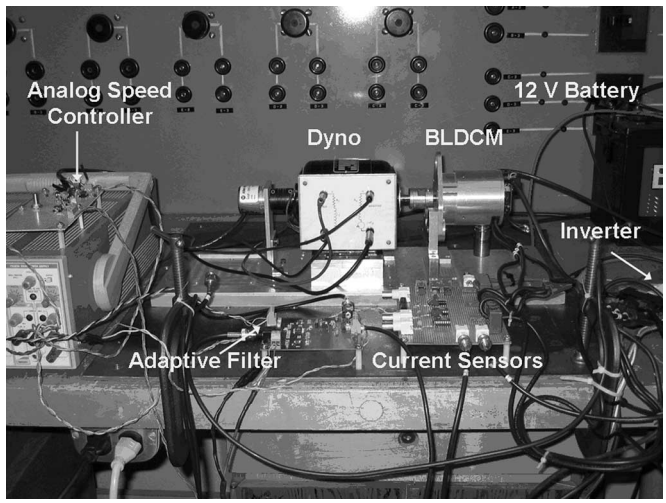

Fig. 4. Experimental arrangement for testing dynamic eccentricity.

the length of the air gap [19]. A dynamic-eccentricity change of 32% in the air gap is usually considered to be moderate and hence has been chosen for this paper to depict the ability of the proposed algorithms to detect even moderate fault conditions.

The experimental arrangement is shown in Fig. 4. The current in one phase of the BLDC motor is acquired using Hall-effect sensors. The fundamental and all harmonics that are above the second harmonic are adaptively filtered out using a switch-capacitor filter that was developed in the laboratory. The notch filter that is used to remove the fundamental is a sixth-order elliptic switch-capacitor filter that is designed using the software FilterCAD from Linear Technologies. Such a high-order filter is designed to obtain a sharp notch that would filter only the fundamental and leave the fault frequencies near the fundamental unaffected. The sixth-order filter is implemented using the LTC1061 high-performance triple universal integrated circuit and provides a notch attenuation of 56 dB. A phase-locked loop is used to track the fundamental frequency from the BLDC Hall position sensor signal and provide the desired clock to the switch-capacitor filter. The filtered and unfiltered currents are sampled at a rate of 2 kHz. A time window of 1 s comprising 2000 samples is used to compute the wavelets. This window is selected to be the largest one possible from a computation aspect as such wavelets are not influenced by the wavelets as long as the number of scales is adequate for representation.

Rapid time-varying motor operation is obtained by varying the BLDC motor speed (ω_M in Fig. 1). Experiments are

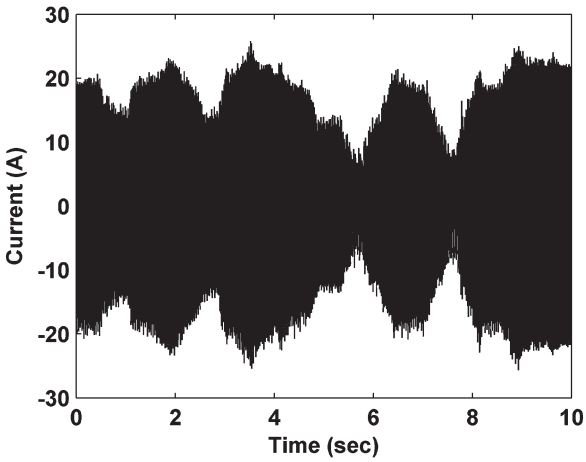

Fig. 5. Nonstationary stator current of a BLDC motor (with dynamic eccentricity).

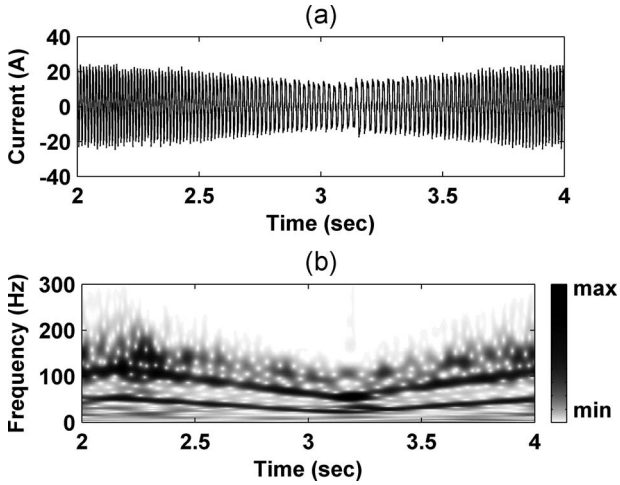

Fig. 6. AWT scalogram of filtered BLDC motor (with dynamic eccentricity) stator current with 5-Hz triangular speed reference.

conducted with sinusoidal, triangular, and randomly changing speed references. The sinusoidal and triangular references vary at a rate of 0–10 Hz, representing most practically occurring applications. The BLDC motor-speed variation ω_M for a sinusoidal speed reference is

$$\omega_M = 5\sin(2\pi f_{\text{ref}} t) \quad \text{where} \quad f_{\text{ref}} \text{ is between 0 and 10 Hz.} \tag{17}$$

The motor is tested under load conditions that vary from full load to low load, depending on the instantaneous speed of operation. This is achieved using a dc generator, which provides full load to the BLDC motor at a rated speed. The full-load stator current for the motor is 20 A.

VII. Experimental Results

The typical stator current of a BLDC motor operating under nonstationary conditions is shown in Fig. 5. For a six-pole BLDC motor, the rotor-fault frequencies occur at 1/3, 2/3, 4/3, and 5/3 times the fundamental frequency, as computed from (15). The AWT-ridge algorithm is implemented in Matlab using the Wavelab802 toolbox from Stanford University [20]. The discrete wavelet version of the AWT is computed at eight scales that are selected as powers of two, i.e., $s^{-1} = \{2, 4, 8, 16, 32, 64, 128, 256\}$. Twelve intermediate scales are also computed between each scale.

Two important parameters of the Gabor wavelet play an important role in determining the quality of the method's time and frequency resolutions, namely: 1) variance σ^2 and 2) wavelet center frequency η. Both these parameters need to be tuned to obtain the best performance. However, for the purpose of demonstrating the proposed AWT-based fault-detection algorithm, variance σ^2 of the analytic Gabor wavelet is initially chosen to be 1. The effect of variance will be further illustrated in Section VIII. Frequency parameter η is then varied arbitrarily to obtain good frequency resolution with as little interference terms as possible. An η of 14 is found to offer good frequency resolution while also maintaining good time resolution.

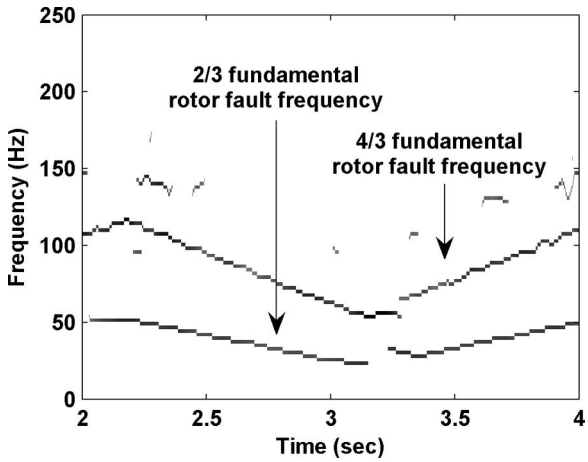

Fig. 7. AWT-ridge extraction from filtered stator current scalogram in BLDC motor operating with 5-Hz triangular speed reference.

The stator current of the dynamically eccentric BLDC motor operating at a 5-Hz triangular speed reference and the scalogram $|Wf(u,s)|^2$ of the filtered stator current that is computed using (3) and (4), as shown in Fig. 2, are shown in Fig. 6. Darker zones in the scalogram represent higher amplitudes. The fault frequencies are not clearly evident in the scalogram. The local maxima (also called the AWT ridges) are then computed from the scalogram, as explained in Fig. 2. These AWT ridges represent the instantaneous eccentricity frequencies of the signal. The instantaneous fault frequencies (AWT ridges) in the filtered stator current, and its corresponding scalogram of Fig. 6, are shown in Fig. 7. The two dynamic-eccentricity frequencies at 2/3 and 4/3 the fundamental frequencies are distinctly seen to vary over time. The ridge algorithm efficiently extracts only the fault frequencies while suppressing noise and other artifacts. The amplitude of these AWT ridges can be used to measure the health of the motor.

The AWT ridges of the filtered stator current of a dynamically eccentric BLDC motor now operating with an 8-Hz triangular speed reference are shown in Fig. 8. The AWT ridges (not shown here for this case) are again extracted from the

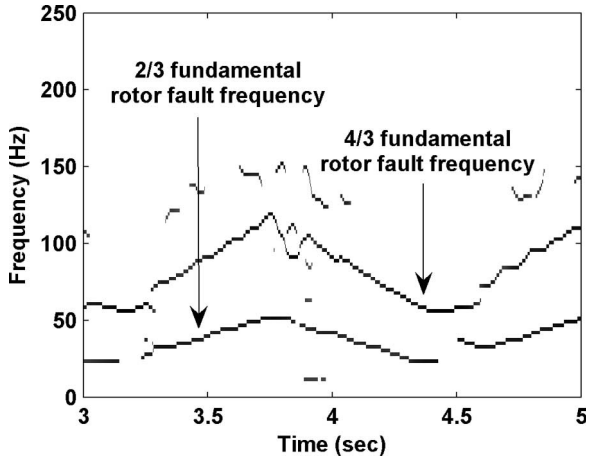

Fig. 8. AWT ridges of filtered stator current in BLDC motor operating with 8-Hz triangular speed reference.

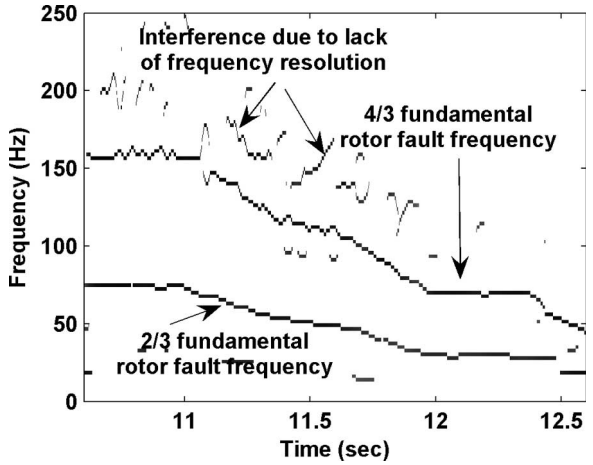

Fig. 9. AWT ridges of filtered stator current in BLDC motor operating with continuous random speed reference.

scalogram computed using (3) and (4) of the filtered stator current, as explained in Fig. 2. A triangular speed variation is a more severe nonstationary operation than a sinusoidal speed reference. It can be seen from Fig. 8 that the AWT fault-detection algorithm is able to track the fault frequencies distinctly over time. Similarly, the AWT fault ridges of the filtered stator current of a dynamically eccentric BLDC motor operating with a random speed reference (Fig. 5) are shown in Fig. 9. Some interference terms are seen to be present in Fig. 9. These interference terms arise as frequency resolution conditions (13) and (14) are not perfectly satisfied for the value of η, which was chosen here to be 14. These components are however small and do not affect rotor-fault classification. Although the interference terms cannot be completely removed, they can be minimized by carefully fine tuning the values of η and σ. The fault ridges are seen to be tracked distinctly over time, thus confirming that AWT is a suitable tool for detecting faults in motors operating under rapidly varying speed conditions.

Once the AWT ridges have been extracted, the last step in a motor dynamic-eccentricity detection algorithm is fault classification (Fig. 1). Several fault classifiers for motor-fault

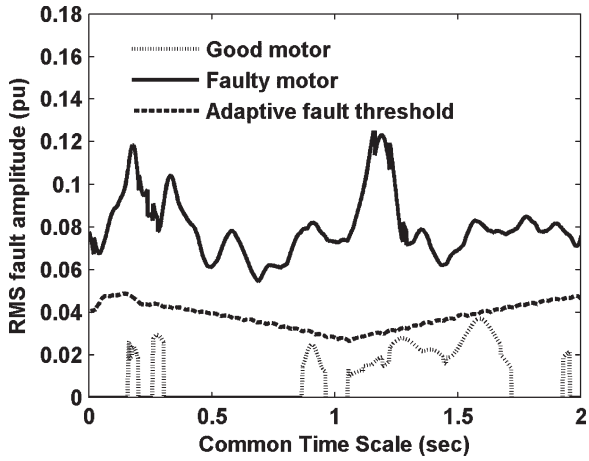

Fig. 10. AWT-ridge-based BLDC rotor-fault detector using rms fault metric.

detection have been researched in the past, and some of these could be used depending on the sophistication needed for a given application [21]. In this paper, a simple fault metric is computed from the amplitudes of the instantaneous fault frequencies (AWT ridges) that are extracted from the scalogram of the filtered stator current. The fault metric is calculated by obtaining the rms value of the AWT-ridge amplitudes for every instant of time using (16). Only the AWT ridges in a selected frequency band are used to calculate the rms value. In the present fault scenario, the rms is calculated for all the ridges in a frequency band of $f_e \pm f_e/2$, where f_e is the fundamental frequency of the BLDC stator current. This fault metric is used in a fault classifier that will indicate a motor fault if the metric is above a preset threshold. Fig. 10 shows the rms fault metrics that are computed from the AWT-ridge amplitudes of the filtered stator currents of a good and a faulty motor operating with a 5-Hz triangular speed reference. A clear difference can be seen in the fault amplitudes between a good and a bad motor. A preset adaptive threshold varies as 2.5% of the fundamental amplitude is set heuristically, i.e.,

$$\text{adaptive threshold} = 0.025 * \text{amplitude}[\text{AWRi}_{\text{aunf}}] \quad (18)$$

where $\text{AWRi}_{\text{aunf}}$ is the analytic wavelet ridge of the unfiltered BLDC current that is computed from the local maxima of the scalogram. It can be seen from Fig. 10 that the adaptive thresholding scheme effectively distinguishes a faulty motor from a good one. A common time scale is used as the stator currents from the good and faulty motors were recorded at different times.

VIII. Comments on the Proposed AWT-Ridge Algorithm

A. AWT and Multiple Fault Discrimination

Every motor has some small abnormality from the time of manufacture and would have some of the fault-frequency components. Hence, in all the condition-monitoring algorithms, base measurements are taken for a good motor prior to commissioning. Once commissioned, the fault algorithm monitors the

amplitudes of the fault frequencies and tracks changes in their amplitudes over time. A significant change in the amplitudes indicates a developing fault. While the case of dynamic eccentricity has been investigated in this paper, the method can be readily extended to several other rotor faults that create unique fault-frequency signatures in the stator-current spectrum. These faults included mixed eccentricity (combined dynamic and static eccentricity), broken rotor faults in induction motors, bearing defects, and load-related defects such as gear faults and coupling misalignments. These faults create unique fault frequencies that have been extensively documented [2]–[4]. The actual type of fault can be determined by correlating the fault frequency to the fundamental frequency value that can also be extracted using the scalogram of the unfiltered stator current. This can be done by monitoring the amplitude of all the fault frequencies individually and determining their relation to the fundamental frequency. If multiple faults produce the same fault frequencies, then actual fault-type discrimination may not be possible. However, in such cases, the extracted frequency information can be used to just indicate the health of the motor, as mentioned in the beginning of this section.

The choice of wavelet affects the fault-detection process significantly. As the rotor faults are low-frequency sinusoidal quantities, smooth wavelets are needed to approximate these components. As a result, sharp discrete wavelets such as Daubechies cannot be used for good accuracy [22]. The smooth continuous wavelets, on the other hand, cannot be easily implemented in practice as discrete versions for many of them are not available. The AWT offers a good compromise and is one of the few wavelets that can be used for motor-fault detection.

B. Selecting AWT Parameters

The frequency resolution of the Gabor analytic wavelet ridge algorithm is dependent on the length of the AWT window and the parameters of the wavelet function, i.e., variance σ^2 and wavelet center frequency η. The influence of wavelet center frequency η is first investigated. The bandwidth conditions (13) and (14) have to be satisfied for good frequency resolution. This means that the AWT-ridge method strongly depends on parameter η, which is the center frequency of the mother wavelet. Equations (13) and (14) depend on the physical phenomena being encountered. The rate and pattern of change of the motor speed have a strong influence on the choice of η. For example, let us assume that the two fault frequencies in the signal of interest vary as two linear chirps [11], i.e.,

$$f(t) = a_1 \cos(bt^2 + ct) + a_2 \cos(bt^2) \quad (19)$$

$$\frac{|\varphi_2'(u) - \varphi_1'(u)|}{\varphi_1'(u)} = \frac{c}{bt}. \quad (20)$$

Equation (20) shows that for a selected time window, parameter η can be calculated to meet the bandwidth conditions. Based on this, a selection process can be recommended.

1) Choose a time window based on the available computational capability.

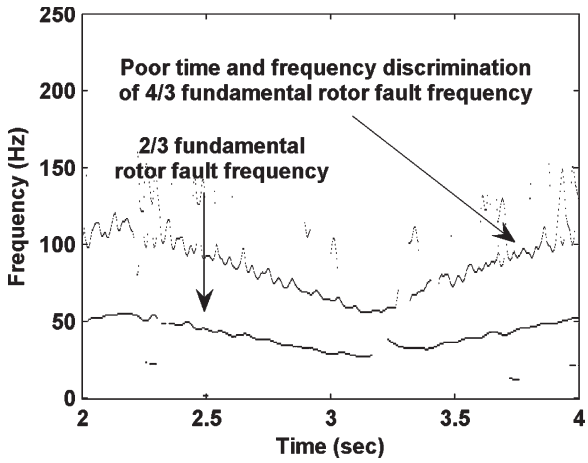

Fig. 11. AWT scalogram of filtered BLDC motor (with dynamic eccentricity) stator current with 5-Hz triangular speed reference ($\eta = 6$ and $\sigma = 1$) depicting poor frequency discrimination.

2) The positive derivative of the phases of all the frequency signals, i.e., φ', is calculated. This may already be available if determination of the stationary phase is used to compute the AWT ridges [from (12)].
3) The value of $\eta(\Delta\omega = 1)$ is then calculated from (13) and (14) as in (20).

As this process increases the computational complexity of the algorithm, a heuristic selection process through trial and error can also be employed. In this paper, η is selected through trial and error as only one fault is considered, and the number of fault frequencies in the signal is known beforehand. In the experimental results of the previous section, η was tuned to 14 (the value of σ^2 is still assumed as 1). Fig. 11 shows the AWT for the same experimental result of Fig. 7 but for a η value of 6 ($\sigma^2 = 1$). The frequency discrimination in Fig. 7 is poor, and there are many interference terms, which underline the importance of selecting the correct value of η.

The Gaussian parameter σ is the standard deviation or the width of the Gaussian. Hence, this parameter directly controls the shape of the wavelet, thereby directly affecting the wavelet transform's time and frequency resolutions. For example, the previous case of the AWT with $\eta = 6$ is again considered for analysis. Standard deviation σ is now increased to 2 ($\sigma^2 = 4$). Fig. 12 now shows the AWT for the same experimental result of Fig. 7 but with the new parameters. The interference terms are almost absent, and the resolution in both the time and frequency is much better. This demonstrates the importance of carefully selecting the standard deviation (or variance) in a Gaussian (Gabor) analytic wavelet. As a suggested guideline, a standard deviation of 1 is usually sufficient for most diagnostic problems, with the center frequency being adjusted to reduce the interference terms. However, in applications requiring larger frequency resolution, a higher standard deviation of 2 may be used.

C. Practical Implementation of the AWT Algorithm

To demonstrate the practical suitability of the proposed fault-detection technique, the AWT is implemented on the ADSP-21369 digital signal processor (DSP) from Analog Devices.

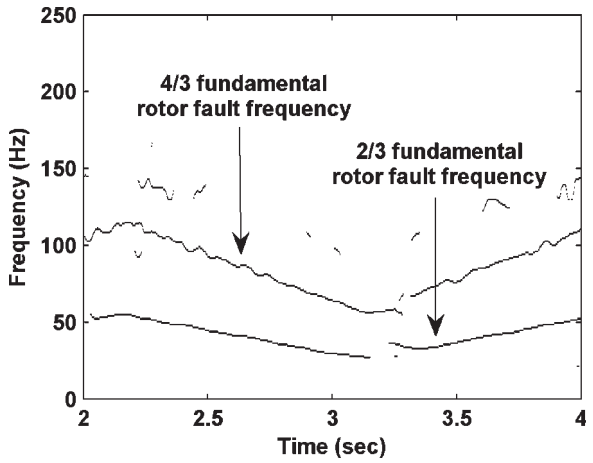

Fig. 12. AWT scalogram of filtered BLDC motor (with dynamic eccentricity) stator current with 5-Hz triangular speed reference ($\eta = 6$ and $\sigma = 2$) depicting better frequency discrimination than Fig. 11.

The ADSP-21369 is a 32-bit floating-point processor with a clock speed of 400 MHz. The processor has a 2-Mb on-chip static random access memory and a 6-Mb user-definable on-chip read-only memory. The development platform has an additional 8 Mb of Flash memory. The algorithm requires 1 239 425 machine cycles to perform the AWT on a 256-long data array, using 4 octaves and 12 voices. The computational time is 3.736 ms for the DSP running at 331.776 MHz. This results in a 256 $\times$ 48 complex array that holds the AWT. This computes to 786 kb of memory requirement (assuming that the complex number is stored as two 32-bit words). This memory requirement is not excessive and is easily manageable in DSP systems today. While the computational time may seem large to be implemented frequently, motor diagnostic is performed over long intervals of time (every 30 min to 1 h). Thus, the computation time may not be very critical, and the proposed algorithm can be implemented as an online diagnostics scheme.

IX. Conclusion

A novel AWT-based detector has been proposed for the detection of dynamic eccentricity in BLDC motors operating under never-steady-state conditions. The method does not need assumption of local stationarity in the signal as wavelets are multiresolution tools that are developed for the analysis of nonstationary signals. Experimental results have shown that the AWT-ridge method can detect dynamic eccentricity under various types of nonstationary motor operation. A fast wavelet algorithm can be used to implement the method in real time. The proposed method is not limited to the detection of only dynamic eccentricity but can also be used for the detection of other faults such as bearing faults. The method can also be used for rotor-fault detection in other types of motors such as induction motors aside from BLDC motors.

Acknowledgment

The authors would like to thank Delphi Corporation, Troy, MI, for the support and, particularly, Dr. T. Sebastian of Delphi Saginaw Steering Systems and Dr. B. Lequesne and Dr. T. W. Nehl of Delphi Research Laboratories for their help.

References

[1] P. Yedamale, "Brushless DC (BLDC) motor fundamentals," *Microchip Technology Application Note-AN885*, pp. 1–20, 2003. [Online]. Available: http://ww1.microchip.com/downloads/en/AppNotes/00885a.pdf

[2] S. Nandi and H. A. Toliyat, "Condition monitoring and fault diagnosis of electrical machines—A review," in *Proc. 34th IEEE Ind. Appl. Soc. Annu. Meeting*, 1999, vol. 1, pp. 197–204.

[3] J. M. Cameron, W. T. Thomson, and A. B. Dow, "Vibration and current monitoring for detecting airgap eccentricity in large induction motors," *Proc. Inst. Electr. Eng.*, vol. 133, no. 3, pp. 155–163, 1986.

[4] D. G. Dorell, W. T. Thomson, and S. Roach, "Analysis of airgap flux, current, and vibration signals as a function of the combination of static and dynamic airgap eccentricity in 3-phase induction motors," *IEEE Trans. Ind. Appl.*, vol. 33, no. 1, pp. 24–34, Jan./Feb. 1997.

[5] M. H. Hayes, *Statistical Digital Signal Processing and Modeling*. New York: Wiley, 1996.

[6] B. Yazici and G. B. Kliman, "An adaptive statistical time-frequency method for detection of broken bars and bearing faults in motors using stator current," *IEEE Trans. Ind. Appl.*, vol. 35, no. 2, pp. 442–452, Mar./Apr. 1999.

[7] K. Kim and A. G. Parlos, "Induction motor fault diagnosis based on neuropredictors and wavelet signal processing," *IEEE/ASME Trans. Mechatronics*, vol. 7, no. 2, pp. 201–219, Jun. 2002.

[8] R. Burnett, J. F. Watson, and S. Elder, "The application of modern signal processing techniques for use in rotor fault detection and location within three-phase induction motors," in *Proc. IEEE IMTC*, 1995, pp. 426–431.

[9] L. Eren and M. J. Devaney, "Motor bearing damage detection via wavelet analysis of the starting current transient," in *Proc. 18th IEEE IMTC*, 2001, pp. 1797–1800.

[10] M. Vetterli and C. Herley, "Wavelets and filter banks: Theory and design," *IEEE Trans. Signal Process.*, vol. 40, no. 9, pp. 2207–2232, Sep. 1992.

[11] S. Mallat, *A Wavelet Tour of Signal Processing*. San Diego, CA: Academic, 1999, pp. 84–88. 102–107.

[12] J. M. Aller, T. G. Habetler, R. G. Harley, R. M. Tallam, and S. B. Lee, "Sensorless speed measurement of AC machines using analytic wavelet transform," *IEEE Trans. Ind. Appl.*, vol. 38, no. 5, pp. 1344–1350, Sep./Oct. 2002.

[13] S. Rajagopalan, W. le Roux, R. G. Harley, and T. G. Habetler, "Diagnosis of potential rotor faults in brushless DC machines," in *Proc. 2nd Int. Conf. PEMD*, 2004, pp. 668–673.

[14] G. B. Kliman and J. Stein, "Methods of motor current signature analysis," *Electr. Mach. Power Syst.*, vol. 20, no. 5, pp. 463–474, Sep. 1992.

[15] B. Ayhan, M.-Y. Chow, and M.-H. Song, "Multiple discriminant analysis and neural-network-based monolith and partition fault-detection schemes for broken rotor bar in induction motors," *IEEE Trans. Ind. Electron.*, vol. 53, no. 4, pp. 1298–1308, Jun. 2006.

[16] J.-H. Jung, J.-J. Lee, and B.-H. Kwon, "Online diagnosis of induction motors using MCSA," *IEEE Trans. Ind. Electron.*, vol. 53, no. 6, pp. 1842–1852, Dec. 2006.

[17] A. Jornet, J. Cusido, A. G. Espinosa, J. A. Ortega, and L. Romeral, "Double frequency test for detecting faults in induction machines," in *Proc. IEEE IECON*, 2005, pp. 1–6.

[18] M. Eltabach, A. Charara, and I. Zein, "A comparison of external and internal methods of signal spectral analysis for broken rotor bars detection in induction motors," *IEEE Trans. Ind. Electron.*, vol. 51, no. 1, pp. 107–121, Feb. 2004.

[19] P. Bechard, "Fault zone analysis 'Air Gap'," in *Proc. Motor Reliab. Tech. Conf.*, 2004, pp. 1–7. [Online]. Available: http://www.pdma.com/AirGapFaultZone.pdf

[20] J. Buckheit, S. Chen, D. Donoho, I. Johnstone, and J. Scargle, *WaveLab Reference Manual*, 1995. Ver 0.7000. [Online]. Available: http://www-stat.stanford.edu/~wavelab/ftp/WaveLabRef.pdf.Z

[21] F. Filippetti, G. Franceschini, C. Tassoni, and P. Vas, "Recent developments of induction motor drives fault diagnosis using AI techniques," *IEEE Trans. Ind. Electron.*, vol. 47, no. 5, pp. 994–1004, Oct. 2000.

[22] B. A. Paya, I. I. Esat, and M. N. M. Badi, "Artificial neural network based fault diagnostics of rotating machinery using wavelet transforms as a preprocessor," *Mech. Syst. Signal Process.*, vol. 11, no. 5, pp. 751–765, Sep. 1997.

Satish Rajagopalan (S'99–M'01) received the B.E. degree in electrical engineering from the University of Madras, Chennai, India, in 1997, the M.S.E.E. degree from Iowa State University, Ames, in 2000, and the Ph.D. degree from the Georgia Institute of Technology, Atlanta, in 2006.

From 2000 to 2001, he was with Baldor Motors and Drives, Fort Smith, AR, as a Power Electronics Engineer, where he was involved in the design of electric motor drives. He is currently a Senior Engineer in the Power Delivery Group, Electric Power Research Institute, Knoxville, TN. His research interests include switching power converter technology, motor control, and motor condition monitoring.

Dr. Rajagopalan is a member of the IEEE Industry Applications, IEEE Power Electronics, and IEEE Industrial Electronics Societies.

José M. Aller was born in Caracas, Venezuela, in 1958. He received the Ing. degree in electrical engineering from the Universidad Simón Bolívar, Caracas, in 1980, the M.S. degree in electrical engineering from the Universidad Central de Venezuela, Caracas, in 1982, and the Ph.D. degree in industrial engineering from the Universidad Politécnica de Madrid, Madrid, Spain, in 1993.

He has been a Lecturer at the Universidad Simón Bolívar for 26 years, where he is currently a Full-Time Professor in the Departamento de Conversión y Transporte de Energía. He was the General Secretary of the Universidad Simón Bolívar from 2001 to 2005. His research interests include space-vector applications, electrical machine control, and power electronics.

José A. Restrepo (S'89–M'92) received the B.Sc. and M.Sc. degrees in electronics engineering from the Universidad Simón Bolívar, Caracas, Venezuela, in 1988 and 1991, respectively, and the Ph.D. degree from the University of Manchester, Manchester, U.K., in 1996.

He is currently a Full Professor of electronics engineering in the Departamento de Conversión y Transporte de Energía, Universidad Simón Bolívar. His research interests include advanced control of electrical machines, artificial intelligence, and digital signal processors applied to motion control.

Thomas G. Habetler (S'83–M'83–SM'92–F'02) received the B.S.E.E. and M.S. degrees in electrical engineering from Marquette University, Milwaukee, WI, in 1981 and 1984, respectively, and the Ph.D. degree from the University of Wisconsin, Madison, in 1989.

From 1983 to 1985, he was with the Electro-Motive Division, General Motors, as a Project Engineer. Since 1989, he has been with the School of Electrical and Computer Engineering, Georgia Institute of Technology, Atlanta, where he is currently a Professor of electrical engineering. He is a regular Consultant in the field of condition-based diagnostics for electrical systems. His research interests include electric machine protection and condition monitoring, switching converter technology, and drives, on which topics he has published more than 150 papers.

Dr. Habetler currently serves as the IEEE Division II Director-Elect. He was the President of the IEEE Power Electronics Society and the Chair of the Industrial Power Converter Committee of the IEEE Industry Applications Society. He is a recipient of four conference prize paper awards from the IEEE Industry Applications Society.

Ronald G. Harley (M'77–SM'86–F'92) received the M.Sc.Eng. degree (*cum laude*) in electrical engineering from the University of Pretoria, Pretoria, South Africa, in 1965, and the Ph.D. degree from London University, London, U.K., in 1969.

In 1971, he was appointed Chair of Electrical Machines and Power Systems at the University of Natal, Durban, South Africa, where he later became the Department Head and the Deputy Dean of Engineering. He is currently the Duke Power Company Distinguished Professor in the School of Electrical and Computer Engineering, Georgia Institute of Technology, Atlanta. He has coauthored some 400 papers, ten of which attracted prizes from journals and conferences. He is the holder of three patents. His research interests include the dynamic behavior and condition monitoring of electric machines, motor drives, power systems and their components, and controlling them by the use of power electronics and intelligent control algorithms.

Dr. Harley is a Fellow of the Institution of Electrical Engineers, U.K., a Fellow of the Royal Society in South Africa, and a Founder Member of the Academy of Science in South Africa, which was formed in 1994. In 2000 and 2001, he was one of the IEEE Industry Applications Society's six Distinguished Lecturers. He was the Vice-President of Operations of the IEEE Power Electronics Society (from 2003 to 2004) and the Chair of the Atlanta Chapter of the IEEE Power Engineering Society. He is currently the Publications Chair for the IEEE Power Electronics Society and the Chair of the Distinguished Lecturers and Regional Speakers program of the IEEE Industry Applications Society. He was a recipient of the Cyrill Veinott Award in 2005 from the IEEE Power Engineering Society for "outstanding contributions to the field of electromechanical energy conversion."